

Intersite Coulomb repulsion driven quadrupole instability and magnetic ordering in the orbital frustrated $\text{Ba}_2\text{MgReO}_6$

Xuanye Zhang,^{1,*} Jinyu Zou,^{1,*} and Gang Xu^{1,2,3,†}

¹Wuhan National High Magnetic Field Center & School of Physics,
Huazhong University of Science and Technology, Wuhan 430074, China

²Institute for Quantum Science and Engineering,

Huazhong University of Science and Technology, Wuhan, 430074, China

³Wuhan Institute of Quantum Technology, Wuhan, 430074, China

We develop an unrestricted Hartree-Fock mean-field method including Coulomb repulsion U , V and spin-orbital coupling λ self-consistently to investigate the mechanism of structural instability and magnetic ordering in $\text{Ba}_2\text{MgReO}_6$. A comprehensive quadrupole phase diagram versus U and V with $\lambda=0.28\text{eV}$ is calculated. Our results demonstrate that, while U and λ mainly lead to the onsite quadrupole $Q_{x^2-y^2}$ and $Q_{3z^2-r^2}$ with orbital frustration, the easy-plane anisotropy or the intersite Coulomb repulsion V can remove the frustration. Finally, the $V>10\text{meV}$ would arrange $Q_{x^2-y^2}$ antiparallely, accompanied with small parallel $Q_{3z^2-r^2}$, and stabilize $\text{Ba}_2\text{MgReO}_6$ into the body centered tetragonal structure. Such antiparallel $Q_{x^2-y^2}$ provides a new mechanism of Dzyaloshinskii–Moriya interaction, and gives rise to the canted antiferromagnetic (CAF) state along $[110]$ axis. Moreover, sizable octupoles such as O_{21}^{31} , O_{21}^{33} , O_{21}^{34} and O_{21}^{36} are discovered for the first time in CAF states. Our study not only provides a comprehensive understanding of the nature and exotic properties in $\text{Ba}_2\text{MgReO}_6$, but also reveals some commonality of 5d compounds.

5d electrons usually have two remarkable characters. One is the dramatically enhanced spin-orbital coupling (SOC) λ originated from the huge atomic number Z . The other is the spatially extended orbital, which could lead to considerable intersite Coulomb repulsion V . In the past decades, the interplay between the energy comparable onsite Coulomb repulsion U and SOC and its resulting exotic properties in 5d transition metal (TM) compounds have attracted increasing interest, including the SOC assistant Mott metal-insulator transition [1–3], non-collinear magnetic moment [4–6], orbital frustration (OF) [7–9] and high-rank multipole [10–15]. Among them, the orbital frustrated honeycomb and face-centered cubic (Fcc) lattice magnets have been extensively studied recently, which are reported to host the long-pursuit quantum spin liquid states when the OF maintains and dominates [16–18], or give rises to lattice distortion accompanied with the orbital ordering (OO) when OF is eliminated [19–22]. However, while most efforts have been focused on the interplay between U and λ and the resulting properties, rare works pay attention to the influence of V , though it could play a key role to determine the exotic states and properties in 5d TM compounds. Especially in the first-principles calculation field, a generic program to deal with U , V and λ self-consistently is still lacking.

The double perovskite $\text{Ba}_2\text{MgReO}_6$ with $5d^1$ configuration, adopting the frustrated fcc lattice, provides an ideal platform to study the interplay between U , λ and V , as well as the resulting exotic properties [23–30]. $\text{Ba}_2\text{MgReO}_6$ undergoes two phase transitions upon cooling, including Fcc–body centered tetragonal (Bct) phase transition at T_q and canted antiferromagnetic (CAF) phase transition with a small gap at T_m [25–29]. Further

synchrotron X-ray diffraction measurements of high-quality single crystals show the tetragonal distortion is enhanced below T_m , which indicates that quadrupoles are coupled with magnetic orders [26]. Recently, magnetic entropy is obtained by subtracting phonon contribution in heat capacity [29], which reflects the degeneracy of the ground state multiplet $N=2$ is different from Ref [25]. These evidences imply that pure spin model is not enough to describe the magnetic mechanism in $\text{Ba}_2\text{MgReO}_6$. In fact, strong SOC not only leads to small magnetic dipole ordering, as small as $0.3\mu_B$ in $\text{Ba}_2\text{MgReO}_6$, but also opens up the possibility of high-rank multipoles [11, 31]. Such high-rank multipoles are usually entangled with the magnetic dipole ordering together and hard to be detected by the conventional experiments [14, 15]. Therefore, a comprehensive understanding of the phase transitions and exotic properties in $\text{Ba}_2\text{MgReO}_6$ remains elusive until now.

In this letter, based on first-principles calculations, we develop an unrestricted Hartree-Fock mean-field method included U , λ and V self-consistently to investigate the nature of phase transition and exotic properties in $\text{Ba}_2\text{MgReO}_6$. Our study demonstrates that, while U and λ are mainly responsible to onsite order parameters such as orbital quadrupoles and magnetic dipoles, the intersite Coulomb repulsion V plays crucial role for their ordering arrangement. Our calculations figure out that the antiparallel (AP) $Q_{x^2-y^2}$ could minimize the intersite Coulomb repulsion mostly. So that small $V=10\text{meV}$ is enough to stabilize $\text{Ba}_2\text{MgReO}_6$ into the Bct structure accompanied with the AP- $Q_{x^2-y^2}$ and small magnitude of parallel $Q_{3z^2-r^2}$ quadrupole. Such quadrupole state with incompletely quenched orbital angular momentum provides a new mechanism of Dzyaloshinskii–Moriya

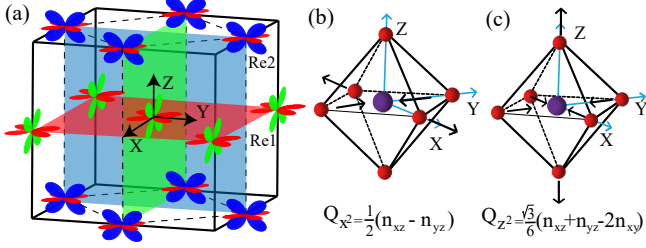


FIG. 1. (a) Schematic of Re1 and Re2 atoms in Fcc unit cell (solid line) and Bct structure (dash lines). XY, XZ and YZ orbital (plane) are indicated by red, green and blue color. (b)(c) The oxygen octahedral distortion modes corresponding to $Q_{x^2-y^2}$ and Q_{z^2} orders.

(DM) interaction, resulting in the experimentally observed CAF ground state [25, 26]. Moreover, various magnetic octupoles are discovered in the CAF ground state, where the octupoles have comparable magnitude with magnetic dipoles and exhibit canted arrangement along [110] direction. This complex magnetic structure may be the source of abnormal magnetic entropy and weak magnetic anisotropy in the CAF ground state.

As shown in Fig. 1a, $\text{Ba}_2\text{MgReO}_6$ adopts double perovskite structure with $Fm\bar{3}m$ space group [23, 25]. The crystal field of the local oxygen octahedron splits d-orbitals of Re atom into higher doubly-degenerate e_g orbitals and lower triply-degenerate t_{2g} orbitals [32, 33]. With $5d^1$ configuration, t_{2g} orbitals are enough for low physics of $\text{Ba}_2\text{MgReO}_6$. The one electron occupation usually leads to spontaneous symmetry breaking with OO [34–38], which can be expanded by the quadrupole orders $Q_{x^2-y^2}$ (abbr. Q_{x^2}) and $Q_{3z^2-r^2}$ (abbr. Q_{z^2})

$$\begin{aligned} Q_{x^2-y^2} &= \frac{1}{2}(n_{xz} - n_{yz}) \\ Q_{3z^2-r^2} &= \frac{\sqrt{3}}{6}(n_{xz} + n_{yz} - 2n_{xy}) \end{aligned} \quad (1)$$

where n_i ($i = xy, xz, yz$) is electron occupation. The Q_{x^2} breaks O_h to D_{2h} and Q_{z^2} breaks to D_{4h} , corresponding to the octahedral distortion shown in Fig. 1b and Fig. 1c respectively.

In order to comprehensively investigate the effects of the interactions, including U , λ and V , on the OO and physical properties in $\text{Ba}_2\text{MgReO}_6$, we first construct the maximally localized non-magnetic (NM) Wannier functions of t_{2g} to obtain H_{tb} , using the Vienna ab initio simulation [39, 40] and WANNIER90 package [41–43] based on the primitive cell of Fcc structure with lattice constant $a = 8.0802 \text{ \AA}$ [26]. Then U , λ and V are successively added to calculate the possible orders and corresponding energy, by self-consistent unrestricted Hartree-Fock mean-field method.

We first take the onsite Coulomb repulsion H_U into account, which adopts the form of Kanamori Hamilto-

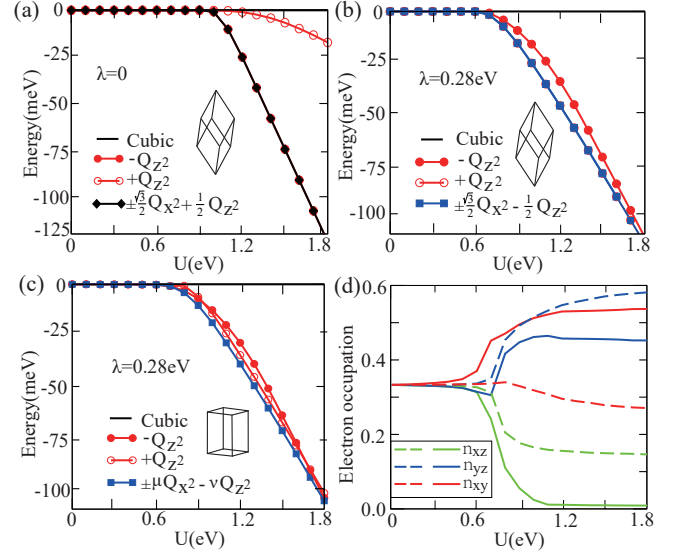


FIG. 2. The total energy of OO states with the parameters $\lambda=0$ (a), $\lambda=0.28 \text{ eV}$ (b) in Fcc primitive cell and $\lambda=0.28 \text{ eV}$ in Bct structure (c). (d) The Re2's electron occupation of d_{xy} , d_{xz} and d_{yz} orbitals in $\text{AP-}Q_{x^2} + Q_{z^2}$ with $V=50 \text{ meV}$ (dash line) and $-\mu Q_{x^2} - \nu Q_{z^2}$ state without V (solid line).

nian [44] and has been reported as the driving force of the OO in many materials [45–49]. The calculated results are shown in Fig. 2a. When $U > 1.0 \text{ eV}$, three symmetrically equivalent quadrupole states $-Q_{z^2}$ ($n_{xy}=1$), $\frac{\sqrt{3}}{2}Q_{x^2} + \frac{1}{2}Q_{z^2}$ ($n_{xz}=1$) and $-\frac{\sqrt{3}}{2}Q_{x^2} + \frac{1}{2}Q_{z^2}$ ($n_{yz}=1$) emerge spontaneously, which are about dozens meV lower than their counterparts with opposite ordering such as Q_{z^2} . One can understand the result by the mean field total energy of the Kanamori Hamiltonian with time-reversal symmetry (TRS):

$$E = -\frac{U}{4}(Q_{x^2-y^2}^2 + Q_{3z^2-r^2}^2) \quad (2)$$

which gives the energy $-\frac{U}{12}$ for $-Q_{z^2}$ state with $n_{xy} = 1$, lower than the energy of Q_{z^2} state ($-\frac{U}{48}$) with $n_{xz}=n_{yz}=0.5$. Such results demonstrate that the onsite Coulomb repulsion U tends to enforce the electron to occupy single orbital.

To reveal the effect of SOC on OO, we further introduce H_{soc} of t_{2g} orbitals [32], which splits real orbitals into higher doublet $|J_{eff} = 1/2\rangle$ and lower quartet $|J_{eff} = 3/2\rangle$ states. The SOC strength $\lambda=0.28 \text{ eV}$ is determined by the NM band structures fitting with first-principles calculations. Obviously contrary to the case without SOC, the results with SOC as plotted in Fig. 2b, identify that Q_{z^2} ($n_{xz}=n_{yz}=0.5$), $\frac{\sqrt{3}}{2}Q_{x^2} - \frac{1}{2}Q_{z^2}$ ($n_{xz}=n_{xy}=0.5$) and $-\frac{\sqrt{3}}{2}Q_{x^2} - \frac{1}{2}Q_{z^2}$ ($n_{yz}=n_{xy}=0.5$) orders become more stable, about 10 meV lower than $-Q_{z^2}$ state in the regime $0.9 \text{ eV} < U < 1.5 \text{ eV}$. These results can be understood by the effect of U in the spin-orbital

entangled quartet states $|J_{eff} = 3/2 \rangle$, which are [32]

$$\begin{aligned} \left| J_{eff} = \frac{3}{2}, m = -\frac{3}{2} \right\rangle &= \frac{1}{\sqrt{2}} |d_{yz\downarrow}\rangle - \frac{i}{\sqrt{2}} |d_{xz\downarrow}\rangle \\ \left| J_{eff} = \frac{3}{2}, m = \frac{3}{2} \right\rangle &= -\frac{1}{\sqrt{2}} |d_{yz\uparrow}\rangle - \frac{i}{\sqrt{2}} |d_{xz\uparrow}\rangle \\ \left| J_{eff} = \frac{3}{2}, m = -\frac{1}{2} \right\rangle &= \frac{1}{\sqrt{6}} |d_{yz\uparrow}\rangle - \frac{i}{\sqrt{6}} |d_{xz\uparrow}\rangle + \sqrt{\frac{2}{3}} |d_{xy\downarrow}\rangle \\ \left| J_{eff} = \frac{3}{2}, m = \frac{1}{2} \right\rangle &= -\frac{1}{\sqrt{6}} |d_{yz\downarrow}\rangle - \frac{i}{\sqrt{6}} |d_{xz\downarrow}\rangle + \sqrt{\frac{2}{3}} |d_{xy\uparrow}\rangle \end{aligned} \quad (3)$$

It is obvious that $|m = \pm 3/2 \rangle$ correspond to Q_{z^2} order while $|m = \pm 1/2 \rangle$ correspond to $-Q_{z^2}$ order. The on-site Coulomb repulsion U , through the nearest neighbor hopping t , can induce the antiferromagnetic (AFM) exchange interaction $J(J > 0)$ between same orbitals and ferromagnetic (FM) exchange interaction $J'(J' < 0)$ between orthogonal orbitals, which have the magnitude of $\frac{t^2}{U}$ (about 10meV). Although the system preserves TRS during the calculations in Fig. 2b, the exchange interactions can play roles through the following TRS invariant two-site Fock states $\Psi_m = |A, m\rangle|B, m\rangle + |A, -m\rangle|B, -m\rangle$ or $\Psi'_m = |A, m\rangle|B, -m\rangle - |A, -m\rangle|B, m\rangle$, with $m = 1/2, 3/2$. Our analytical calculations find that while J cannot distinguish $m=1/2$ and $m=3/2$ subspace, J' could make $m=3/2$ subspace lower. By making up the interactions between same orbitals from J term [50], the FM exchange term can be rewritten as

$$J' S_i^t S_j^t = J' \sum_{\sigma=x,y,z} S_i^{\sigma} S_j^{\sigma} \quad (4)$$

where S_j^t is the total spin at j site. Our calculation shows that $\Psi_{m=1/2}$ and $\Psi_{m=3/2}$ have the same energy $\frac{J'}{4}$, while $\Psi'_{m=3/2}$ and $\Psi'_{m=1/2}$ are split with $\frac{-J'}{4}$ and $\frac{-J'}{4} - \frac{2J'}{9}$ respectively. These results clearly reveal that the electron favors the lower $|m = \pm 3/2 \rangle$ subspace, which gives Q_{z^2} quadrupole state. Notice that, $\pm \frac{\sqrt{3}}{2} Q_{x^2} - \frac{1}{2} Q_{z^2}$ states are equivalent to Q_{z^2} state due to the cubic symmetry, and the OF still remains.

In order to release the restriction of cubic symmetry and investigate the possible OO, we further perform our calculations in the Bct structure, as shown by the dash line in Fig. 1a. This super structure has the same lattice as the cubic but with the vector $Q=2\pi(001)$, which has been widely reported in double perovskite materials[51–55]. The calculated results in Fig. 2c demonstrate the splitting between Q_{z^2} state (about 8 meV higher) and $\pm\mu Q_{x^2} - \nu Q_{z^2}$ states ($\mu \neq \frac{\sqrt{3}}{2}$ and $\nu \neq \frac{1}{2}$), suggesting that the electron in this system tends to occupy d_{xy} orbital. This result implies that $\text{Ba}_2\text{MgReO}_6$ has the easy-plane anisotropy, which is included in the H_{tb} already. Such anisotropy can be reflected by the electron occupation in Fig. 2d, which is uniform (1/3) for the three orbitals in the small U regime, but is enhanced to

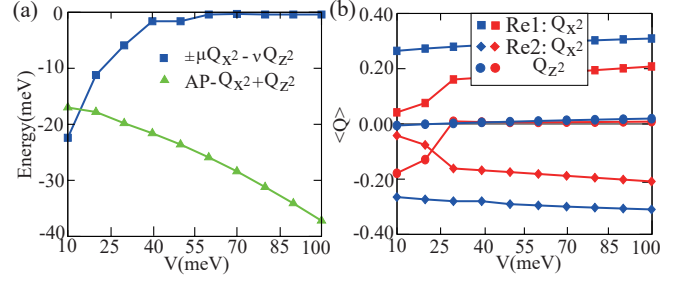


FIG. 3. (a) The energy of $\pm\mu Q_{x^2} - \nu Q_{z^2}$ and $AP-Q_{x^2} + Q_{z^2}$ states as function of V at $U=1.0\text{eV}$ and $\lambda=0.28\text{eV}$, with respect to cubic phase. (b) Evolution of quadruple orders of $AP-Q_{x^2} + Q_{z^2}$ state with V increasing. Red and blue represent the NM and CAF magnetic ground states, respectively.

over 0.5 for d_{xy} orbital with U increasing, illustrating the partially breaking of OF.

In the next, we take the intersite Coulomb repulsion into account with the form $H_V = V \sum_{\alpha} \sum_{\langle ij \rangle \in \alpha} [\frac{4}{3}(n_{i,\beta} - n_{i,\gamma})(n_{j,\gamma} - n_{j,\beta}) + \frac{4}{9}n_{i,\alpha}n_{j,\alpha}]$ ($\alpha, \beta, \gamma = XY, YZ, ZX$ and $\alpha \neq \beta \neq \gamma$), which usually reaches hundred meV in 5d compounds [31, 56] and is reported to play critical role for the quadrupoles [23, 30]. The energy and orders of quadrupole states versus V are shown in Fig. 3a & 3b with $U = 1.0\text{eV}$ and $\lambda=0.28\text{eV}$. With V increasing, the energy of $\pm\mu Q_{x^2} - \nu Q_{z^2}$ states is soon close to cubic phase, while another new quadrupole state with $AP-Q_{x^2}$ and small $+Q_{z^2}$ order is stabilized.

Such results can be reflected by the electron occupation of Re atoms in $AP-Q_{x^2} + Q_{z^2}$ state with $V=50\text{meV}$, as shown in Fig. 2(d). Compared to the $V=0$ case (solid line), the d_{xy} occupation (dash red line) is decreased. On the other hand, V imposes electron of Re1 to occupy d_{xz} orbital while electron of Re2 to occupy d_{yz} orbital, as schematically shown in Fig. 1a. This is because such OO in $AP-Q_{x^2} + Q_{z^2}$ state can maximally reduce the intersite Coulomb repulsion. As shown in Fig. 2d, since n_{xy} is less than 1/3 at $V=50\text{meV}$, a local positive Q_{z^2} with small magnitude is induced on Re1 and Re2 as shown in Fig. 3b. These results clarify that $|m = \pm 1/2 \rangle$ replaces $|m = \pm 3/2 \rangle$ to become the dominant state when $V > 10\text{meV}$. As a result, the presence of V further removes OF in cubic and stabilizes the quadrupole ground state $AP-Q_{x^2} + Q_{z^2}$. These discussion provides a profound understanding about experimentally reported structural instability and OO in $\text{Ba}_2\text{MgReO}_6$.

We further calculate the quadrupole phase diagram based on Bct structure with $\lambda = 0.28\text{eV}$, as shown in Fig. 4a. The phase I without OO (green) is in small U regime, whereas $U > 0.7\text{eV}$ regime shows phase II with $\pm\mu Q_{x^2} - \nu Q_{z^2}$ orders (blue) for small V , and phase III with $AP-Q_{x^2} + Q_{z^2}$ orders (red) for $V > 10\text{meV}$, which indicates that the anisotropy of $\text{Ba}_2\text{MgReO}_6$ is about 10meV.

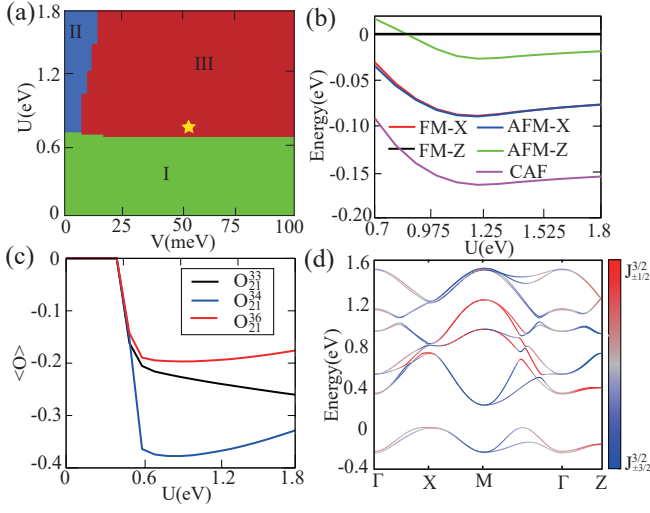


FIG. 4. (a) The quadrupole phase diagram with respect to U and V . Region I, II, and III represent cubic, $\pm\mu Q_{x^2} - \nu Q_{z^2}$, and AP- $Q_{x^2} + Q_{z^2}$ states, respectively. $\text{Ba}_2\text{MgReO}_6$ is located at the position marked by the yellow star. (b) Total energy of magnetic states relative to FM-Z. (c) The magnitude of Re1's octupoles in CAF ground state, including O_{21}^{33} , O_{21}^{34} and O_{21}^{36} . (d) Band structures of CAF ground state at $U=0.8\text{eV}$, $V=50\text{meV}$.

The OO in AP- $Q_{x^2} + Q_{z^2}$ state can drive a special magnetic structure, i.e., CAF. We rewrite quadrupole Q_{x^2} using the angular momentum operator $Q_{x^2} = \frac{1}{2}(L_x^2 - L_y^2)$, where $L_x = id_{xz}^\dagger d_{xy} + h.c.$ and $L_y = id_{xy}^\dagger d_{yz} + h.c.$ [11]. Yielding to AP- Q_{x^2} orders, the L_x and L_y on two Re atoms are exchanged ($L_{x,y}$ of Re1 \leftrightarrow $L_{y,x}$ of Re2), connected by a glide mirror symmetry $\{M_{110}|(0, a/2, a/2)\}$. Thus, the angular momentums form a canted angle which, as SOC is considered, provides a new mechanism of DM interactions $\sum_{\langle i,j \rangle} D(S_i \times S_j)$ in spin space [57–59]. This interaction is an intrinsic property of OF, and induces the CAF with [110] easy-axis as discussed below.

Our self-consistent magnetic calculations confirm that the CAF state is 50 meV lower than other magnetic states including FM-Z, FM-X, AFM-Z and AFM-X states, as shown in Fig. 4b at $\lambda=0.28\text{eV}$ and $V=50\text{meV}$. The result also shows significant energy difference (about 50meV) between X-orientated and the Z-orientated magnetic states, which is much larger than the typical magnetocrystalline anisotropy energy. Such anomaly may be originated from the distinct quadrupoles and octupoles in the magnetic states with different symmetries.

The CAF state in $\text{Ba}_2\text{MgReO}_6$ exhibits rich magnetic multipole physics including dipoles and octupoles. For the former, the ratio between $L_x + 2S_x$ ($0.258\mu_B$) and $L_y + 2S_y$ ($0.117\mu_B$) of Re1 is approximately 2.2 in the CAF ground state, leading to $0.283\mu_B$ magnetic moment with canted angle $\phi \sim 20^\circ$ along [110] direction, which agrees well with the experimentally measured $0.3\mu_B$, $\phi \sim 40^\circ$ [26]. In addition, CAF state also has considerable

TABLE I. The magnitude of magnetic octupoles at $\lambda=0.28\text{eV}$, $U=0.8\text{eV}$ and $V=50\text{meV}$ in CAF ground state.

	O_{21}^{31}	O_{21}^{33}	O_{21}^{34}	O_{21}^{36}
Re1	-	-0.2213	-0.3772	-0.1961
Re2	-0.3772	0.1961	-	0.2213

octupoles including O_{21}^{31} , O_{21}^{33} , O_{21}^{34} and O_{21}^{36} . We plot the evolution of octupoles on Re1 with increment of U in Fig. 4c, in which the magnitude of O_{21}^{34} and O_{21}^{36} reduce slowly, whereas O_{21}^{33} increases. By exchanging L_x and L_y in the expression of octupoles, we obtain the relationship of the octupoles on the two Re atoms as $O_{21}^{31}(\text{Re2}) = O_{21}^{34}(\text{Re1})$ and $O_{21}^{33}(\text{Re1}) = -O_{21}^{36}(\text{Re2})$, as listed in Table I. It reveals that AP- Q_{x^2} makes octupoles also have a canted ordering. Since the magnitude of octupoles is as large as dipoles, they should have a significant impact on the electronic structures and physical properties of $\text{Ba}_2\text{MgReO}_6$. How to detect such canted octupoles is an interesting and important question waiting for addressing in the future.

In Fig. 3b, we compare the quadrupole order of the NM and CAF state, which unveils that the magnitude of Q_{x^2} in the CAF ground state is enhanced. This result illustrates the further enhancement of tetragonal distortion in the magnetic phase, which well coincides with the increment of quadrupoles below T_m reported in experiment [26].

In Fig. 4d, by using $U=0.8\text{eV}$, $\lambda=0.28\text{eV}$ and $V=50\text{meV}$, we obtain the band structures of CAF ground state, which gives rise to a Mott insulating state and the band gap of 0.2eV agree well with the experimental observation (0.17eV) [25]. The projection in Fig. 4d also demonstrates that the occupied bands have more $|J_{eff} = 3/2, m = \pm 1/2\rangle$ (red) components than $|J_{eff} = 3/2, m = \pm 3/2\rangle$ (blue), which confirms our previous analysis again. We use these fitting parameters to determine the position of $\text{Ba}_2\text{MgReO}_6$ in the quadrupole phase diagram as shown by the yellow star in Fig. 4a, which is close to the phase boundary between phase III and phase I. This result gives a possible explanation of the quadrupole vanishing and magnetic phase transition under pressure in $\text{Ba}_2\text{MgReO}_6$ [60], which also indicates that similar phase transition may be induced by the substitution or magnetic field.

In summary, we consider U , λ and V in the self-consistent calculations for the first time to investigate the phase transition mechanism and ground state properties in $\text{Ba}_2\text{MgReO}_6$. The onsite U and λ are mainly responsible for the emergence of three equivalent quadrupole states Q_{z^2} , $\frac{\sqrt{3}}{2}Q_{x^2} - \frac{1}{2}Q_{z^2}$ and $-\frac{\sqrt{3}}{2}Q_{x^2} - \frac{1}{2}Q_{z^2}$, reflecting the nature of the OF in the Fcc structure. Such OF can be lifted by the anisotropy or intersite Coulomb repulsion V . Our calculations demonstrate that $\pm\mu Q_{x^2} - \nu Q_{z^2}$

states are 8meV lower than the Q_{z^2} state in the Bct structure, suggesting the native easy-plane anisotropy favors d_{xy} occupation. The effect of V is opposite to that of the easy-plane anisotropy, which will suppress the d_{xy} occupation and lead to the alternative majority of d_{yz} and d_{xz} orbitals along [001] direction. As a result, the system is stabilized in the AP- $Q_{x^2} + Q_{z^2}$ quadrupole state when V is larger than 10meV. We uncover that this AP- Q_{x^2} ordering can induce DM interaction between Re1 and Re2 and finally results in the CAF ground state along [110] direction, consistent with the experiments very well. Besides, our calculations discover the additional octupoles O_{21}^{31} , O_{21}^{33} , O_{21}^{34} and O_{21}^{36} in the CAF state, which also present canted angle with considerable magnitude. These results build up a profound understanding between the interactions and the structural instability, magnetic properties, as well as octupoles in $\text{Ba}_2\text{MgReO}_6$. The program developed in this work provides a generic powerful first-principles tool for accurate investigation of other 5d TM compounds.

Acknowledgments — The authors thank Xi Dai, Yilin Wang, Zhida Song, Jianzhou Zhao, Wenxuan Qiu and Aiyun Luo for valuable discussion. This work was supported by the National Key Research and Development Program of China (2018YFA0307000), and the National Natural Science Foundation of China (12274154).

* These authors made equal contributions to this work.

† e-mail address: gangxu@hust.edu.cn

- [1] B. J. Kim, H. Jin, S. J. Moon, J.-Y. Kim, B.-G. Park, C. S. Leem, J. Yu, T. W. Noh, C. Kim, S.-J. Oh, J.-H. Park, V. Durairaj, G. Cao, and E. Rotenberg, *Phys. Rev. Lett.* **101**, 076402 (2008).
- [2] B. J. Kim, H. Ohsumi, T. Komesu, S. Sakai, T. Morita, H. Takagi, and T. Arima, *Science* **323**, 1329 (2009).
- [3] J. Jeong, B. Lenz, A. Gukasov, X. Fabrèges, A. Sazonov, V. Hutanu, A. Louat, D. Bounoua, C. Martins, S. Biermann, V. Brouet, Y. Sidis, and P. Bourges, *Phys. Rev. Lett.* **125**, 097202 (2020).
- [4] H. Shinaoka, S. Hoshino, M. Troyer, and P. Werner, *Phys. Rev. Lett.* **115**, 156401 (2015).
- [5] S. M. Disseler, C. Dhital, A. Amato, S. R. Giblin, C. de la Cruz, S. D. Wilson, and M. J. Graf, *Phys. Rev. B* **86**, 014428 (2012).
- [6] A. S. Erickson, S. Misra, G. J. Miller, R. R. Gupta, Z. Schlesinger, W. A. Harrison, J. M. Kim, and I. R. Fisher, *Phys. Rev. Lett.* **99**, 016404 (2007).
- [7] C. Wu, *Phys. Rev. Lett.* **100**, 200406 (2008).
- [8] M. V. Mostovoy and D. I. Khomskii, *Phys. Rev. Lett.* **89**, 227203 (2002).
- [9] G. Khaliullin, D. Churchill, P. P. Stavropoulos, and H.-Y. Kee, *Phys. Rev. Res.* **3**, 033163 (2021).
- [10] W. Witczak-Krempa, G. Chen, Y. B. Kim, and L. Balents, *Annu. Rev. Condens. Matter Phys.* **5**, 57 (2014).
- [11] Y. Wang, H. Weng, L. Fu, and X. Dai, *Phys. Rev. Lett.* **119**, 187203 (2017).
- [12] W.-X. Qiu, J.-Y. Zou, A.-Y. Luo, Z.-H. Cui, Z.-D. Song, J.-H. Gao, Y.-L. Wang, and G. Xu, *Phys. Rev. Lett.* **127**, 147202 (2021).
- [13] D. D. Maharaj, G. Sala, M. B. Stone, E. Kermarrec, C. Ritter, F. Fauth, C. A. Marjerrison, J. E. Greedan, A. Paramekanti, and B. D. Gaulin, *Phys. Rev. Lett.* **124**, 087206 (2020).
- [14] L. Zhao, D. Torchinsky, H. Chu, V. Ivanov, R. Lifshitz, R. Flint, T. Qi, G. Cao, and D. Hsieh, *Nat. Phys.* **12**, 32 (2016).
- [15] T. Liang, T. H. Hsieh, J. J. Ishikawa, S. Nakatsuji, L. Fu, and N. P. Ong, *Nat. Phys.* **13**, 599 (2017).
- [16] J. c. v. Chaloupka, G. Jackeli, and G. Khaliullin, *Phys. Rev. Lett.* **105**, 027204 (2010).
- [17] L. Balents, *Nature* **464**, 199 (2010).
- [18] Y. Yamaji, Y. Nomura, M. Kurita, R. Arita, and M. Imada, *Phys. Rev. Lett.* **113**, 107201 (2014).
- [19] D. Khomskii and M. Mostovoy, *J. Phys. A* **36**, 9197 (2003).
- [20] R. Cong, R. Nangneri, B. Rubenstein, and V. F. Mitrović, *Phys. Rev. B* **100**, 245141 (2019).
- [21] K. Oikawa, T. Kamiyama, H. Kato, and Y. Tokura, *J. Phys. Soc. Jap.* **72**, 1411 (2003), <https://doi.org/10.1143/JPSJ.72.1411>.
- [22] B. Yuan, J. P. Clancy, J. A. Sears, A. I. Kolesnikov, M. B. Stone, Z. Yamani, C. Won, N. Hur, B. C. Jeon, T. W. Noh, A. Paramekanti, and Y.-J. Kim, *Phys. Rev. B* **98**, 214433 (2018).
- [23] T. Takayama, J. Chaloupka, A. Smerald, G. Khaliullin, and H. Takagi, *J. Phys. Soc. Jap.* **90**, 062001 (2021).
- [24] K. G. Bramnik, H. Ehrenberg, J. K. Dehn, and H. Fuess, *Solid State Sci.* **5**, 235 (2003).
- [25] D. Hirai and Z. Hiroi, *J. Phys. Soc. Jap.* **88**, 064712 (2019).
- [26] D. Hirai, H. Sagayama, S. Gao, H. Ohsumi, G. Chen, T.-h. Arima, and Z. Hiroi, *Phys. Rev. Res.* **2**, 022063 (2020).
- [27] A. Mansouri Tehrani and N. A. Spaldin, *Phys. Rev. Mater.* **5**, 104410 (2021).
- [28] S. W. Lovesey and D. D. Khalyavin, *Phys. Rev. B* **103**, 235160 (2021).
- [29] J. Pásztorová, A. M. Tehrani, I. Živković, N. A. Spaldin, and H. M. Rønnow, arXiv preprint [arXiv:2210.13616](https://arxiv.org/abs/2210.13616) (2022).
- [30] C. Svoboda, W. Zhang, M. Randeria, and N. Trivedi, *Phys. Rev. B* **104**, 024437 (2021).
- [31] G. Chen, R. Pereira, and L. Balents, *Phys. Rev. B* **82**, 174440 (2010).
- [32] G. L. Stamokostas and G. A. Fiete, *Phys. Rev. B* **97**, 085150 (2018).
- [33] S. Maekawa, T. Tohyama, S. E. Barnes, S. Ishihara, W. Koshibae, and G. Khaliullin, *Physics of transition metal oxides*, Vol. 144 (Springer Science & Business Media, 2004).
- [34] K. I. Kugel and D. Khomskii, *Soviet Physics Uspekhi* **25**, 231 (1982).
- [35] T. Suzuki, M. Katsumura, K. Taniguchi, T. Arima, and T. Katsufuji, *Phys. Rev. Lett.* **98**, 127203 (2007).
- [36] I. S. Elfimov, V. I. Anisimov, and G. A. Sawatzky, *Phys. Rev. Lett.* **82**, 4264 (1999).
- [37] M. Kargarian, J. Wen, and G. A. Fiete, *Phys. Rev. B* **83**, 165112 (2011).
- [38] K. Kugel and D. Khomskii, *Zh. Eksp. Teor. Fiz* **64**, 1429 (1973).
- [39] G. Kresse and J. Furthmüller, *Phys. Rev. B* **54**, 11169

- (1996).
- [40] G. Kresse and J. Furthmüller, *Comput. Mater. Sci.* **6**, 15 (1996).
- [41] *Comput. Phys. Commun.* **185**, 2309 (2014).
- [42] A. A. Mostofi, J. R. Yates, Y.-S. Lee, I. Souza, D. Vanderbilt, and N. Marzari, *Comput. Phys. Commun.* **178**, 685 (2008).
- [43] N. Marzari, A. A. Mostofi, J. R. Yates, I. Souza, and D. Vanderbilt, *Rev. Mod. Phys.* **84**, 1419 (2012).
- [44] A. Georges, L. d. Medici, and J. Mravlje, *Annu. Rev. Condens. Matter Phys.* **4**, 137 (2013).
- [45] H.-T. Jeng, G. Y. Guo, and D. J. Huang, *Phys. Rev. Lett.* **93**, 156403 (2004).
- [46] H.-T. Jeng, G. Y. Guo, and D. J. Huang, *Phys. Rev. B* **74**, 195115 (2006).
- [47] S. Sarkar, T. Maitra, R. Valentí, and T. Saha-Dasgupta, *Phys. Rev. Lett.* **102**, 216405 (2009).
- [48] H.-T. Jeng, G. Y. Guo, and D. J. Huang, *Phys. Rev. Lett.* **93**, 156403 (2004).
- [49] H.-T. Jeng, S.-H. Lin, and C.-S. Hsue, *Phys. Rev. Lett.* **97**, 067002 (2006).
- [50] The superexchange antiferromagnetic and ferromagnetic interaction Hamiltonian is $H = \sum_{\alpha} \sum_{\langle ij \rangle \in \alpha} (J S_{i\alpha} S_{j\alpha} + J' S_{i\alpha} \sum_{j\alpha' \neq \alpha} S_{j\alpha'})$, where $J > 0$, $J' < 0$, and $\alpha = XY, YZ, XZ$. By reorganizing these two terms, the interaction Hamiltonian can be rewritten as, $H = \sum_{\langle ij \rangle} [(J - J') \sum_{\alpha} S_{i\alpha} S_{j\alpha} + J' (\sum_{\alpha} S_{i\alpha}) (\sum_{\alpha} S_{j\alpha})]$. The second term is the effective ferromagnetic interaction we adopt in the main text.
- [51] S. Gao, D. Hirai, H. Sagayama, H. Ohsumi, Z. Hiroi, and T.-h. Arima, *Phys. Rev. B* **101**, 220412 (2020).
- [52] K. Yamamura, M. Wakeshima, and Y. Hinatsu, *J. Solid State Chem.* **179**, 605 (2006).
- [53] A. S. Erickson, S. Misra, G. J. Miller, R. R. Gupta, Z. Schlesinger, W. A. Harrison, J. M. Kim, and I. R. Fisher, *Phys. Rev. Lett.* **99**, 016404 (2007).
- [54] K. E. Stitzer, M. D. Smith, and H.-C. zur Loye, *Solid State Sci.* **4**, 311 (2002).
- [55] R. Morrow, A. E. Taylor, D. Singh, J. Xiong, S. Rodan, A. Wolter, S. Wurmehl, B. Büchner, M. Stone, A. Kolesnikov, *et al.*, *Sci. Rep.* **6**, 1 (2016).
- [56] O. Nagai and T. Nakamura, *Prog. Theor. Phys.* **24**, 432 (1960).
- [57] H. Katsura, N. Nagaosa, and A. V. Balatsky, *Phys. Rev. Lett.* **95**, 057205 (2005).
- [58] T. Moriya, *Phys. Rev.* **120**, 91 (1960).
- [59] I. Dzyaloshinsky, *J. Phys. Chem. Solids* **4**, 241 (1958).
- [60] H. Arima, Y. Oshita, D. Hirai, Z. Hiroi, and K. Matsubayashi, *J. Phys. Soc. Jap.* **91**, 013702 (2022).